

CHAPTER 4

Development of a high sensitivity polarimeter

Applications of polarimetry can be seen in many areas such as; optics, astronomy, nuclear physics and radar. Of particular interest in polarimetry is the accuracy and the speed of measuring the SOP. In this thesis polarimetry is used to measure the change of the SOP in optical elements, from which the birefringence and DGD (if the wavelength is varied) can be determined. One of the main points in this chapter will be the theoretical error analysis for polarimetry. This analysis will be useful for the polarimetric OTDR in Chapter 7.

The structure of this chapter is as follows. Section 4.1 describes, in general, the different state of polarisation and birefringence measurement methods. Section 4.2 reviews the single-channel retarder-analyser combination for measuring the SOP, which will be used in Chapter 7, for the polarimetric OTDR. Section 4.3 treats the optical design and calibration of the real time Stokes polarimeter, developed at University of Essex. Section 4.4 considers the expected error in the measured SOP due to noise, and the inaccuracy in the alignment of the analysing components for the Essex polarimeter. This result will be useful for Chapter 7 where the SOP is measured by a polarimetric OTDR, and the measured intensity is relatively close to the noise floor. In Section 4.5 the measured polarisation matrices of different optical components such as a polarisation independent beamsplitter, $\lambda/8$ plate and two optical fibres, in the forward and forward-backward directions are shown.

4.1 Polarisation and birefringence measurement methods

4.1.1 SOP measurement methods

The state of polarisation for monochromatic light as introduced in Chapter 1 can be completely described by specifying four quantities: the magnitudes and phases of the electric fields in the two orthogonal directions (Jones vector). For the general case of partially polarised light, the four Stokes parameters can be used to describe the light, if the absolute phase information is not required. SOP measurement methods are based on the Stokes parameters because they measure the intensity of the received lightwave. There are various

types of instruments which can measure the SOP, for example, using an adjustable combination of retarder and analyser; polarisation-modulating elements; and interferometry.

The *retarder-analyser combination* changes the relative phase of the received light by the use of a rotatable retardation plate before analysing the intensity by means of a polariser and detector. At least four intensities at different retarder angle positions must be measured to determine the Stokes parameters. The retarder analyser combination is probably the simplest of the SOP measurements as it contains only one moving part. However, this limits the measurement speed. This idea may be extended to a four-channel retarder-analyser combination by splitting the light beam in four parts. No moving parts are involved and the measurement speed is then only limited by the electronics used in the receivers. In Reference [148] such a four-channel polarimeter was used as an active feedback system, together with fibre squeezers to stabilise the output SOP of a fibre.

The *polarisation-modulation polarimeter* is similar to the retarder analyser combination but instead of rotating the retarder the compensator retardance is varied, for example, by electro-optical induced birefringence (Subsection 3.3.7), and the analyser has to be rotated to two different positions (usually 0° and 45°). Although this requires only two polariser positions accurate retardation tuning is difficult to achieve.

The *interferometric method*, based on a modified Michelson interferometer similar to that shown in Figure 3.22, works by inserting polarisers in the two interferometer arms and in front of the receiver [149]. The advantage of this method is the absence of the retardation plate, such that there are no wavelength dependent components requiring calibration. On the other hand, the rotating polarisers and moving mirror have to be adjusted mechanically, thus slowing down the system [149]. A more complex interferometric set-up, having a heterodyne interferometric polarimeter, with a frequency shift in one of the interferometric arms, can display the measured SOP directly on an oscilloscope [150].

4.1.2 Birefringence measurement methods

In this section a short overview of different birefringence measurement methods for optical fibres will be given. Several methods have been proposed which cover different birefringence ranges:

- (i) Birefringence has been measured in short lengths of fibres using different input SOPs (e.g. rotatable polariser), and measuring-analysing the output SOP (simple polarimetric

methods). Various approaches have been used: zeroing the retardation of the fibre by using a rotatable linear polariser at the input and either a Soleil-Babinet compensator - analyser combination [151], [152], or photo-elastic modulator combination at the output [153], characterising the polarisation ellipticity with a rotatable polariser - analyser combination [152], [153], or measuring the fibre matrix using standard polarimetry techniques (Section 4.5). For all these methods the net birefringence $\delta\beta l$ has to be smaller than 2π (π if the fast or slow axis are not known) otherwise there are multiple beats of the polarisation modes and the fibre has to be cut-back to determine the birefringence [103].

- (ii) The modulation of the intrinsic birefringence by a known amount can be used to measure the birefringence either by using electro-optic or magneto-optic modulation of the SOP on a small section of fibre [154], [37], and analysing the output SOP, which can also give information about the local circular birefringence; or by applying variable twist to the fibre [155], [156], or lateral pressure on HiBi fibres [157], [150], which modifies the birefringence via the elasto-optic effect (Subsection 3.3.3).
- (iii) The fibre birefringence has been estimated from the measured polarisation mode dispersion in short length of fibres (no random mode coupling) in the frequency domain [79], [158], [159], in the time domain, using short pulses measuring the flight time difference between the two output pulses [160], or by using the interferometric method [161] (see Section 3.5 for more detailed discussion of the PMD measurement methods). Although as discussed in Chapter 3 the group delay and phase delay in a fibre are not the same, and can vary from fibre to fibre depending on parameters such as core diameter, doping levels, centre wavelength, etc. (see Section 3.3). The difference between the DGD and differential phase delay has been shown in some HiBi fibres (mainly stress birefringence) to be between 10 to 20% [158], whereas the low birefringence fibres (typical telecommunication fibres with contributions from shape and stress birefringence) show a discrepancy of $\sim 50\%$ in measurements and simulation results (see Subsection 3.3.2 and Subsection 7.5.1)
- (iv) Rayleigh scattering intrinsically manifested in the optical fibre can be used to measure birefringence:
 - 1) By direct visualisation of the beat length from a side view of the fibre using visible light ($\lambda \sim 0.6 \mu\text{m}$) [152]. Rayleigh scattering is in all directions except along the dipole axis of the scatterer. If equal power is launched into both PEMs of the fibre, the inter-modal beating can be observed. This method is limited to the visible light range because of the λ^{-4} dependence of scattered light and to HiBi fibres (beat lengths around a few millimetres) where the beat visibility (bright and dark bands) give the best contrast.

- 2) By the use of polarisation OTDR, [16] an extension to OTDR [17]. The polarisation information contained in the backscattered light from a pulse propagating along the fibre can be extracted by polarimetry to calculate not only the linear birefringence along the fibre, but also the circular birefringence [15]. Chapter 7 will be mainly devoted to POTDR measurement results and analysis. The smallest measurable beat length, which is twice the minimum spatial resolution, in our POTDR measurements is determined by the pulsewidth, ($L_{b,min} > 2$ m for a 10 ns pulsewidth).
- (v) The local birefringence may be estimated by measuring the ellipticity of the fibre core and cladding (see Section 3.3) e.g. using a far field measurement or preform analyser (see Appendix C), although the stress in the fibre has to be measured [162], to get a complete description of the net local birefringence in the fibre as discussed in Section 3.3. In Reference [81], the measured short length polarisation dispersion, which relates to the birefringence (iii), has been found to be in good agreement with measured core ellipticity and stress in the fibre.

There are many different birefringence measurement methods as discussed above but polarisation OTDR is unique in the sense that it can measure birefringence with access to only one end and is non-destructive.

4.2 Polarimetry principles revisited

4.2.1 The general compensator analyser polarimeter

The simplest polarimeter with the least amount of components is the general compensator analyser (GCA). In Figure 4.1 a sketch of a GCA is shown with a rotatable compensator, e.g. a $\lambda/4$ retardation plate and either a fixed or rotatable analyser (polariser), and optical detection, for example, commercially available power meter. The intensity I as measured by the detector shown in Figure 4.1 can be obtained by consecutive multiplication of the Mueller matrices of the individual components. Assuming an ideal receiver (no polarisation sensitivity), the total intensity per data point defined by the top row of the resultant Mueller matrix for the optical system as shown in Figure 4.1 is

$$I(b,d,a) = [1 \ 0 \ 0 \ 0] \mathbf{M}_A(b,d) \mathbf{M}_C(a) \bar{\mathbf{S}} \quad (4.1)$$

where \mathbf{M}_C and \mathbf{M}_A are the Mueller matrices for the compensator and analyser respectively.

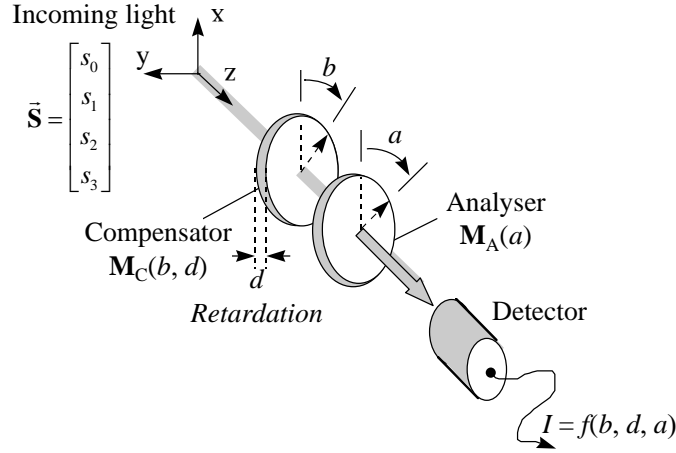


Figure 4.1 Sketch of general compensator analyser polarimeter set-up

For an ideal compensator-analyser the Mueller matrices are [28]

$$\mathbf{M}_A(a) = \frac{1}{2} \begin{bmatrix} 1 & \cos(2a) & \sin(2a) & 0 \\ \cos(2a) & \cos^2(2a) & \cos(2a)\sin(2a) & 0 \\ \sin(2a) & \cos(2a)\sin(2a) & \sin^2(2a) & 0 \\ 0 & 0 & 0 & 0 \end{bmatrix}$$

$$\mathbf{M}_C(b, d) = \begin{bmatrix} 1 & 0 & 0 & 0 \\ 0 & A \sin^2(d/2) + \cos^2(d/2) & B \sin^2(d/2) & -C \sin(d) \\ 0 & B \sin^2(d/2) & -A \sin^2(d/2) + \cos^2(d/2) & D \sin(d) \\ 0 & C \sin(d) & -D \sin(d) & \cos(d) \end{bmatrix}$$

$$A = \cos(4b), B = \sin(4b), C = \sin(2b), D = \cos(2b)$$
(4.2)

where a is the angle of the polariser, d is the retardation and b the angular orientation of the fast axis of the retarder. The measured intensity given in Equation (4.1) is a scalar per data point and combined with Equation (4.2) can be written as a function of the input SOP as

$$\begin{aligned} I(b, d, a) = & \frac{1}{2} (S_0 + S_1(\cos(2a - 2b)\cos(2b) - \cos(d)\sin(2b)\cos(2a - 2b)) + \\ & + S_2(\cos(2a - 2b)\sin(2b) + \cos(d)\cos(2b)\sin(2a - 2b)) + \\ & + S_3(\sin(d)\sin(2a - 2b))) \end{aligned} \quad (4.3)$$

In order to determine the SOP, the intensity has to be measured for at least four independent compensator-analyser positions. These are independent if the SOPs which are allowed through the ideal GCA combination are not located on a great circle on the Poincaré sphere. The four measured intensities can be written as an intensity vector $\vec{\mathbf{I}}$ whose elements are related to the input SOP by Equation (4.3) which contains four linear independent equations and can be written as a constant 4×4 transfer matrix \mathbf{M}_T

$$\vec{\mathbf{I}}(b,d,a) = \mathbf{M}_T(b,d,a)\vec{\mathbf{S}} \quad \text{or} \quad \vec{\mathbf{S}} = \mathbf{M}_T^{-1}\vec{\mathbf{I}} \quad (4.4)$$

From the measured intensities and the inverse of the transfer matrix \mathbf{M}_T , the SOP of the light can be calculated. It is known from matrix calculation that in order to take the inverse the transfer matrix, Equation (4.4) has to be non-singular, this requirement is satisfied if the compensator analyser positions are chosen to be independent of each other as mentioned above.

4.3 Development of a high sensitivity wide dynamic range four-channel polarimeter

4.3.1 Optical design of Essex polarimeter

In a real time polarimeter the light beam is split into four which when passed through four different GCA combinations can be used to calculate the SOP (Equation (4.4)). The light beam may be split using either beamsplitters or by expanding the light beam using a collimator lens so that the four GCA combinations are illuminated directly. The former method is used in the four-channel POTDR (Chapter 7) whilst the latter method is used in the Essex polarimeter. In Figure 4.2 a sketch of the Essex polarimeter is shown with fibre input to a collimator lens, which illuminates the four different polarisation filters before the four Stokes components are measured in four optical detectors simultaneously. The four measured intensities are then amplified, digitised and transferred to a personal computer where the SOP is calculated.

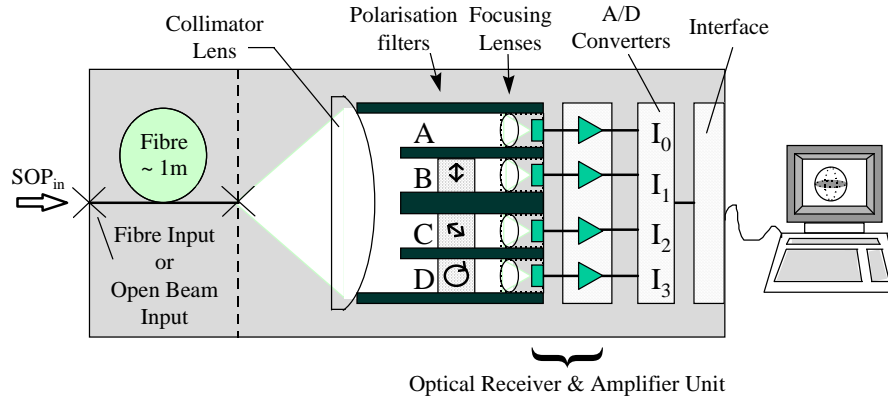


Figure 4.2 Block schematic of Essex polarimeter

The polarimeter has been also designed for open beam input using a fibre collimator at the input, instead of the fibre connector, which allows the measurement of absolute SOPs with the polarimeter. The fibre between the fibre input and the collimator lens is necessary in order to keep the wavefront illuminating the four-channels constant. In Appendix D there are some photographs of the Essex polarimeter. In Table 4.1 the polarisation filters used are listed, and have been chosen in this way in order to keep the polarimeter transfer matrix away from singularity, and also to minimise the number of optical components and wavelength sensitivity of the $\lambda/4$ plate.

Channel	Filter	Values
A (I_0)	no filter	
B (I_1)	polariser	$a_1 = 90^\circ$
C (I_2)	polariser	$a_2 = -45^\circ$
D (I_3)	RCP ¹ $\lambda/4$ plate + polariser	$d_3 = \lambda/4$, $b_3 = 0^\circ$ $a_3 = -45^\circ$

Table 4.1 Nominal values of the polarisation filters in the four-channels.

The general structure of the different filters used in the Essex polarimeter gives the expression for the transfer matrix \mathbf{M}_T as

¹ Right circular polariser (RCP) with $\lambda/4$ plate with fast axis at $b = 0^\circ$ and polariser at $a = -45^\circ$ so that right circular polarised light is transmitted without loss.

$$\mathbf{M}_T = \frac{1}{2} \begin{bmatrix} 2 & 0 & 0 & 0 \\ 1 & \cos(2a_1) & \sin(2a_1) & 0 \\ 1 & \cos(2a_1) & \sin(2a_1) & 0 \\ 1 & C & D & E \end{bmatrix} \quad (4.5)$$

$$C = \cos(2a_3 - 2b_3) \cos(2b_3) - \cos(d_3) \sin(2b_3) \sin(2a_3 - 2b_3)$$

$$D = \cos(2a_3 - 2b_3) \sin(2b_3) - \cos(d_3) \cos(2b_3) \sin(2a_3 - 2b_3)$$

$$E = \sin(d_3) \sin(2a_3 - 2b_3)$$

Inserting the nominal values in Table 4.1 in Equation (4.5) the resultant transfer matrix is

$$\mathbf{M}_T = \frac{1}{2} \begin{bmatrix} 2 & 0 & 0 & 0 \\ 1 & -1 & 0 & 0 \\ 1 & 0 & -1 & 0 \\ 1 & 0 & 0 & -1 \end{bmatrix} \quad \mathbf{M}_T^{-1} = \begin{bmatrix} 1 & 0 & 0 & 0 \\ 1 & -2 & 0 & 0 \\ 1 & 0 & -2 & 0 \\ 1 & 0 & 0 & -2 \end{bmatrix} \quad (4.6)$$

4.3.2 Advantages and disadvantages of a four-channel polarimeter

As mentioned before the main advantage of a four-channel polarimeter as shown in Figure 4.2 is that there are no mechanical rotating components involved thus improving the reliability and accuracy compared to the one channel polarimeter in Figure 4.1. Further more the bandwidth is only limited by the electrical receiver allowing fast sampling of the SOP which is important in systems where the SOP is changing rapidly with time.

There are also some disadvantages, such as the increased power loss caused by splitting the light in the four paths, which gives a minimum expected loss of 6 dB. The total measured loss by using three beam splitters (Chapter 7, four-channel POTDR), is about 9 dB and for the large collimated beam illuminating the four-channels, the measured loss is about 13 dB. Both losses include intrinsic and alignment losses. The loss of ~13 dB in the Essex polarimeter is inherent to the geometry as can be seen from Figure 4.3, which shows clearly

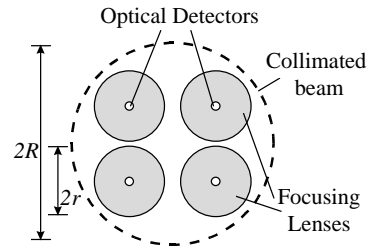


Figure 4.3 Front view from optical subsystem of Essex polarimeter, $2R = 24$ mm and $2r = 8.5$ mm.

that not all the intensity of the large collimated beam can be focused into the four detectors. A source of inaccuracy affecting the four-channel polarimeter is drift in the receiver units with time and temperature, and some polarisation sensitivity if using polarisation beam splitters (see Tables 4.3 and 4.4).

4.3.3 The electrical units of the polarimeter

The electrical unit in Figure 4.2 consists of three consecutive conversions which are; the optical input power conversion into an electrical photo current; the amplification and voltage conversion by the preamplifier; and the digitising by a 16 bit analogue-to-digital converter. A receiver unit with low noise, high stability, low offset drifts and large dynamic range has been developed by the MSc student, Tobias Ernst, Dr. Stuart Walker of University of Essex and myself, in order to have a highly accurate polarimeter for SOP measurements. The final performance characteristics of the polarimeter are listed in Table 4.2 and a detailed description of the receiver development with noise analysis (considering shot noise and Johnson/thermal noise) can be found in the MSc report from Ernst [163].

Wavelength operating range	1.2 μm to 1.6 μm
Input power range	+10 to -70 dBm
Average power measurement linearity	$\pm < 0.6$ dB
SOP uncertainty on Poincaré sphere representation ^{2,3}	$< \pm 2^\circ$
DOP measurement uncertainty ^{2,3}	$\pm 2\%$
Measurement rate	max. 2 kHz

Table 4.2 Polarimeter performance characteristics

4.3.4 Calibration of the polarimeter

4.3.4.1 Linearising the four-channels of the polarimeter

A small difference in the gain and some small non-linearity in the four-channels over the large dynamic range of 80 dB made it necessary to linearise the four-channels relative to each other. In Figure 4.4(a) the set-up used for linearising the polarimeter is shown. The polarimeter is connected to a laser by an optical attenuator and 3 dB coupler. The attenuation is increased by computer control and the measured powers in the four-channels are compared and linearised by a look-up table in the software programme, using the power measured by the reference power meter. This allowed absolute calibration of the polarimeter.

² for input power > -50 dBm, from 1.48 to 1.56 μm with 100% polarised light.

³ averaged over 200 sample points.

4.3.4.2 The transfer matrix of the polarimeter

The transfer matrix of the polarimeter as given in Table 4.1 assumes the ideal position of the polarisers angles, quarter wave plate angle and retardation. In practise this is quite difficult to achieve and there will be an error associated with the relative angles of the components to each other. We would expect that the error in the relative polariser position in the optical head is $< 1^\circ$ from the nominal values given in Table 4.1 (As specified from the manufacturer of the optical head). There will be also an error in the retardation of the quarter wave plate⁴ at the specified wavelength of $1.55 \mu\text{m}$, which is less than $\pm 1.5\%$ in the $\lambda/4$ plate used for calibration of the polarimeter, shown next. However, because this error in the alignment of the polarisers is not acceptable for the SOP measurement, a calibration procedure for the polarimeter has been devised to minimise this error.

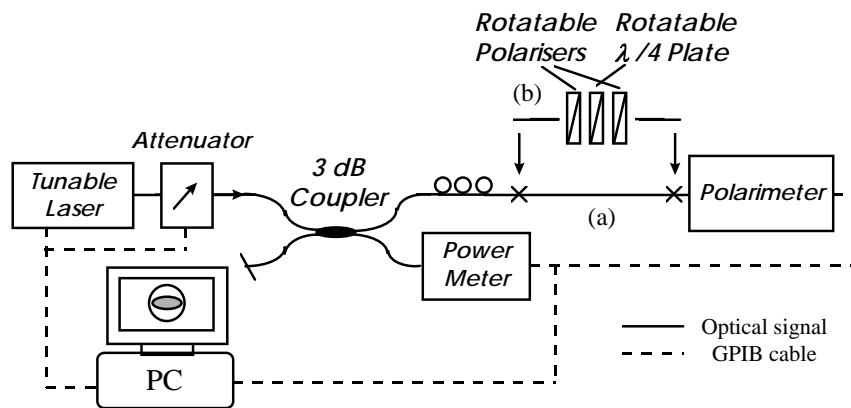


Figure 4.4 Set-up used for calibration of polarimeter.

The calibration set-up to obtain the transfer matrix of the polarimeter, is shown in Figure 4.4(b). The output light of the tunable laser source is set to the specified wavelength e.g. at $1.55 \mu\text{m}$, and after passing through the polarisation controller to allow maximum power transfer through the polariser- $\lambda/4$ -polariser combination, is inserted into the polarimeter. The alignment of the axes of the polariser- $\lambda/4$ -polariser combination are the crucial point in the set-up to generate the well-defined SOPs. The set-up as indicated, uses an open beam with the first polariser as the reference polariser (fixed), and the $\lambda/4$ plate and the polariser which are mounted in a motorised rotary stage from Newport [164]. Both can be controlled manually over a motion controller, or over GPIB from the computer and the minimum step size is specified by Newport as 0.001° with an accuracy of $\pm 0.05^\circ$ [164]. With the rotary stage, it is possible to align the fast axis of the $\lambda/4$ plate and the last polariser very accurately to the axis

⁴ The quarter wave plate used are zero order wave plates designed for $1.55 \mu\text{m}$. Zero order wave plates are insensitive to temperature changes and moderately insensitive to a wavelength change.

of the first polariser, by crossing the two polarisers and searching for the maximum extinction ratio. In the crossed polariser position by a successive interplay of small rotations of the $\lambda/4$ plate and the second polariser, an extinction ratio > 50 dB could be achieved, ensuring exact alignment of the polariser- $\lambda/4$ plate- polariser axes, and the error in alignment is only limited by the accuracy (or smallest step size) of the rotation stages.

With the aligned polarisers-quarter wave plate axes, it is now possible to generate well defined SOPs. The linear SOPs along the equator of the Poincaré sphere are generated by rotating the second polariser (see Figure 4.5) with the $\lambda/4$ plate at 45° to generate circularly polarised light at the input of the rotating polariser, so that the output power remains constant. For the generation of elliptical SOPs, the second polariser is removed, Figure 4.4, and the $\lambda/4$ plate is rotated. The SOP as a function of rotation, traces a figure of eight on the Poincaré sphere, as shown in Figure 4.5, with circularly polarised light at $\pm 45^\circ$ rotation. The solid lines in Figure 4.5 for the rotating $\lambda/4$ plate and polariser, have been computed using the Mueller matrices for the polariser and $\lambda/4$ plate given in Equation (4.2).

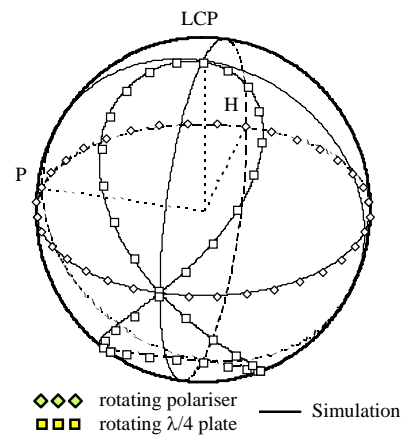


Figure 4.5 Measured SOP with polarimeter, for rotating polariser and $\lambda/4$ plate with 5° step size (see Figure 4.4).

In theory, four independent input SOPs generated from the rotating polariser and the rotating $\lambda/4$ plate are sufficient to calculate the polarimeter transfer matrix. By using more input SOPs, which could be easily obtained by the computer controlled rotary stages as shown in Figure 4.5, the elements of the transfer matrix could be improved by using a least square identification [165]. The off-set of the $\lambda/4$ plate at wavelengths different than designed has to be considered in the calibration. The retardation change in the relevant wavelength range from 1470 to 1570 nm can be very well approximated by the linear equation $\delta\beta_l = \delta\beta_0 \cdot \lambda_0 / \lambda_l$, where $\delta\beta_0 = \pi/2$ at the design wavelength λ_0 and λ_l , is the used wavelength. In Section 4.4 the random and systematic errors in the measured SOP from the polarimeter will be considered.

4.3.5 Review of the one channel polarimeter

A cheaper polarimeter can, as previously stated, be designed by using the GCA shown in Figure 4.1 in combination with an accurate large dynamic range commercial power meter with GPIB. The rotation stages used allow a maximum rotation speed of $7^\circ/\text{sec}$, which, if we just use four different positions of the quarter wave plate (the minimum number to analyse the SOP) within the range 0 to 180° , the total measurement time (with data transfer from power meter over GPIB), is < 45 sec. Care should be taken in the alignment of the collimators with the optical components for the following two reasons:

- (i) Firstly the loss is minimised. In the collimators used with a ~ 0.5 mm beam diameter an intrinsic loss below 3 dB including polariser and $\lambda/4$ plate could be achieved.
- (ii) Secondly any beam deflection caused by rotation of the optical component resulting in a power fluctuation has to be avoided, otherwise an error will result in the estimated SOP. Beam deflection can be minimised by aligning the components rotation axes parallel to the collimated light beam, and by minimising the distance between the collimators. In doing so the rotation of the $\lambda/4$ plate has shown negligible power fluctuation due to beam deflection (below 0.1 dB). The beam deflection from the polariser however, was not less than 0.5 dB in many trials, and was the main reason why the polariser in our GCA system as used in Chapter 7 for the single-channel POTDR is not rotated in order to analyse the SOP.

In Reference [166] it was suggested that in order to minimise the error for a polarimeter system involving a quarter wave plate with polariser, there exists a set of angles where the error due to the relative angular positions between the optical elements and the random fluctuation in the detected intensity, is minimised. The four optimum rotation angles for a rotating quarter wave plate after [166] are at $\alpha = 0, 45^\circ, 75^\circ$ and 95° . In Chapter 7 the single-channel GCA is used for POTDR to analyse the SOP where the $\lambda/4$ plate has been rotated to 18 separate positions, in steps of 10° . The SOP was then calculated from the measured intensities by a least square identification [165], which improved the calculated SOP considerably, due to noise reduction in the individual Stokes components, compared to just using the four analyser positions as suggested above.

4.4 Error analysis in polarimetry

In the measurement of the SOP with a polarimeter, either using a single-channel or four-channels, the measurement errors may be categorised into *systematic* and *random errors*. Systematic errors can arise from the optics, mechanics and from the electronics in the polarimeter, and lead to a constant error in the position of the SOP on the Poincaré sphere.

- (i) *In the optics* these errors can arise from the retardation inaccuracy of the $\lambda/4$ plate at the specified wavelength, from wrongly determining the retardation change with wavelength and from polarisation sensitivity of the receiver, e.g. if the polariser is rotated or if the extinction ratio of the polarisers is not very high. The last two are unimportant because the polarisers used have large extinction ratios (> 40 dB), and the polariser is normally fixed, whereas the first two have to be considered as the specified error in retardation, d , in the $\lambda/4$ plate designed for $\lambda = 1.55 \mu\text{m}$, as $< \pm 1.5\%$ ($\Delta d < 1.4^\circ$).
- (ii) *In the mechanics* due to improper alignment of the polariser-quarter wave plate axes including the four-channel polarimeter, although these elements are fixed. With the calibration procedure described above the alignment accuracy of the axes of the polarisers-quarter wave plate combination is given by the resolution of the rotary stage, which is $\pm 0.05^\circ$. Further, as said above in analysing the SOP with the one channel polarimeter, beam deviation with rotation can lead to an error in the estimated SOP, but this is quite small if the system is properly aligned, and the distance between the collimators is small.
- (iii) *In the electronics*, the errors arise mainly due to non-linearities in the receiver and/or amplifier unit (units), but can also arise due to a drift in the gain of the amplifier which is normally slow in time compared to the measurement time. Non-linearities can be reduced by calibrating the polarimeter versus input power (see Subsection 4.3.4) using an accurate reference power meter with high linearity.

Often the absolute SOP is not so important, as for example in a birefringence or PMD measurement, where only the relative rotation of the output SOP as a function of input SOP or wavelength is of interest. The error in the relative SOP results mainly from the fluctuating random errors in the set-up.

Random errors may be caused by noise or offset drift in the receiver, or possibly due to some vibration in the mechanics. However, they can be also caused by random SOP fluctuation with time in the fibre under test, if e.g., the fibre is not at rest and the SOP changes quickly compared to the measurement time. These errors, especially the receiver noise at low input powers, are the biggest contribution and they cause a spreading in the measured SOP. In general, random noise can be reduced, to some degree, by repeating the measurement over many times and averaging, which is especially important for OTDR (POTDR) where the backscattered power is often < -60 dBm. (Chapter 7)

Next, a first order model will be derived which will be useful for polarimetry in relating the error in the SOP to the systematic error in the optics (for example retardation error of $\lambda/4$ plate), and the error due to receiver noise. These are the two dominant error sources in the polarimeters used (see also polarimetric OTDR in Chapter 7), where the systematic error leads to a constant offset in the measured SOP on the Poincaré sphere, whereas the random error causes an increase in the diameter of the spot representing the SOP on the Poincaré sphere. In order to estimate the expected resultant error in the polarimeter, Equation (4.4) can be re-written as

$$\bar{\mathbf{I}} + \Delta\bar{\mathbf{I}} = (\mathbf{M}_T + \Delta\mathbf{M}_T)(\bar{\mathbf{S}} + \Delta\bar{\mathbf{S}}) \quad (4.7)$$

where $\Delta\bar{\mathbf{I}}$, $\Delta\mathbf{M}_T$ and $\Delta\bar{\mathbf{S}}$ are the errors around their nominal values. Equation (4.5) which determines the polarimeter transfer matrix \mathbf{M}_T can be expanded into a first order Taylor series around the nominal values given in Table 4.1 as

$$\begin{aligned} \Delta I_0 &= \Delta S_0 \\ \Delta I_1 &= \frac{1}{2}(\Delta S_0 - \Delta S_1 - 2\Delta a_1 S_2) \\ \Delta I_2 &= \frac{1}{2}(\Delta S_0 - \Delta S_2 + 2\Delta a_2 S_1) \\ \Delta I_3 &= \frac{1}{2}(\Delta S_0 - \Delta S_3 + S_2 \Delta d_3 + 2(\Delta a_3 - \Delta b_3) S_1) \end{aligned} \quad (4.8)$$

where Δa_i , Δb_i and Δd_i are the errors in radians. Solving the list of linear equations given in Equation (4.8) with respect to $\Delta\bar{\mathbf{S}}$ yields

$$\begin{aligned} \Delta S_0 &= \Delta I_0 \\ \Delta S_1 &= \Delta I_0 - 2\Delta I_1 - 2\Delta a_1 S_2 \\ \Delta S_2 &= \Delta I_0 - 2\Delta I_2 + 2\Delta a_2 S_1 \\ \Delta S_3 &= \Delta I_0 - 2\Delta I_3 + \Delta d_3 S_2 + 2(\Delta a_3 - \Delta b_3) S_1 \end{aligned} \quad (4.9)$$

Dividing the left and right hand side of Equation (4.9) by $\sqrt{S_1 + S_2 + S_3}$, allows visualisation of the error on the surface of the Poincaré sphere, and will normalise the error in the intensities

$$\begin{aligned}
\Delta s_0 &= \frac{\Delta I_0}{I_0} \frac{1}{DOP} \\
\Delta s_1 &= \frac{\Delta I_0}{I_0} \frac{1}{DOP} - \frac{\Delta I_1}{I_0} \frac{2}{DOP} - 2\Delta a_1 s_2 \\
\Delta s_2 &= \frac{\Delta I_0}{I_0} \frac{1}{DOP} - \frac{\Delta I_2}{I_0} \frac{2}{DOP} + 2\Delta a_2 s_1 \\
\Delta s_3 &= \frac{\Delta I_0}{I_0} \frac{1}{DOP} - \frac{\Delta I_3}{I_0} \frac{2}{DOP} + \Delta d_3 s_2 + 2(\Delta a_3 - \Delta b_3) s_1
\end{aligned} \tag{4.10}$$

where $s_i = S_i / \sqrt{S_1 + S_2 + S_3}$ and $DOP = \sqrt{S_1 + S_2 + S_3} / S_0$ as defined in Equation 2.10. Equation (4.10) shows that the error in the Stokes components increases if the light is not fully polarised ($DOP < 1$). The error $\Delta \bar{s}$ of the ideal Stokes vector \bar{s} can be visualised on the Poincaré sphere by an error cone, such that the error is within the semi-aperture angle ε of the cone as shown in Figure 4.6

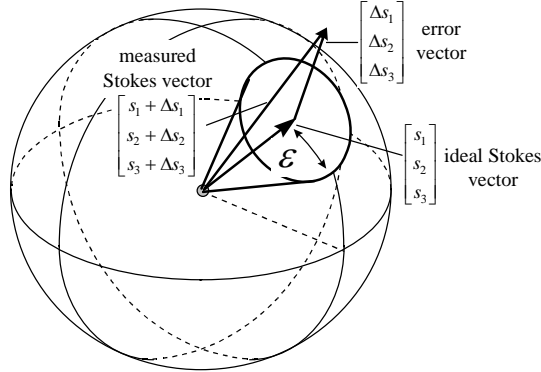


Figure 4.6 Error cone opening indicated on the Poincaré sphere

The opening angle ε can be calculated from Equation (4.10) by using the scalar product $(\bar{s} + \Delta \bar{s}) \cdot \bar{s} = \|\bar{s} + \Delta \bar{s}\| \|\bar{s}\| \cos(\varepsilon)$ where $\|\dots\|$ indicates the norm of the given argument. Rearranging yields

$$\cos(\varepsilon) = \frac{1 + s_1 \Delta s_1 + s_2 \Delta s_2 + s_3 \Delta s_3}{\sqrt{1 + 2(s_1 \Delta s_1 + s_2 \Delta s_2 + s_3 \Delta s_3) + \Delta s_1^2 + \Delta s_2^2 + \Delta s_3^2}} \tag{4.11}$$

The uncertainty in the measured SOPs as displayed in Figure 4.6 is also mirrored in the measured degree of polarisation DOP_M which can be calculated from Equation (4.10) as

$$DOP_M = \frac{\sqrt{(s_1 + \Delta s_1)^2 + (s_2 + \Delta s_2)^2 + (s_3 + \Delta s_3)^2}}{1/DOP + \Delta s_0} \quad (4.12)$$

where DOP without subscript, as used in Equation (4.10), is the actual DOP of the light. Equation (4.12) will be of some interest for Chapter 7 when measuring the backscattered SOP using POTDR.

Next, the errors ε and DOP_M , as given in Equation (4.11) and (4.12) have been calculated as a function of the normalised Stokes vector \bar{s} , for an error in the optical elements of $\Delta a_i = 0.5^\circ$, $\Delta b_3 = 0.5^\circ$ and $\Delta d_3 = \lambda/4 \times 1.5\%$. These are about the errors we would expect in the optics of the Essex polarimeter. The angle of the error cone has been calculated in the presence of noise ΔI_i , which is the RMS value of the noise term and is expressed in noise equivalent optical power (NEP). The signal-to-noise ratio (SNR), at the average optical input power level I_{opt} is defined as

$$SNR = 10 \log(I_{opt}/NEP) = 10 \log(I_0/\Delta I_i) \quad (dB_{opt}) \quad (4.13)$$

Figure 4.7(a) shows the error in the angle ε as a function of \bar{s} at a SNR of 20 dB for fully polarised light. It can be seen that depending on the SOP the error in ε can be up to 3° , although the average error over all the possible SOPs is $\langle \varepsilon \rangle = 1.2^\circ$. The total error in the SOP and measured DOP is a complicated function of the true SOP and analysing optics (Equations 4.11 and 4.12), hence the asymmetry of the shapes in Figure 4.7 arising from the particular chosen polariser and $\lambda/4$ plate positions.

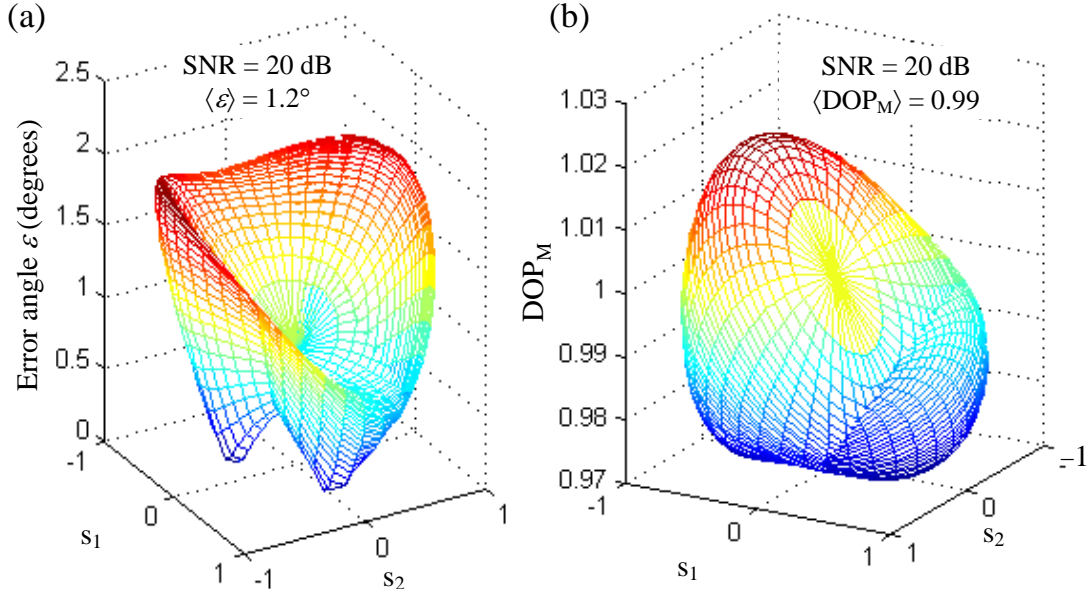


Figure 4.7 Error in measured SOP for fully polarised light with $\Delta a_i = 0.5^\circ$, $\Delta b_3 = 0.5^\circ$ and $\Delta d_3 = \lambda/4 \times 1.5\%$ ($s_3 = \sqrt{1 - s_1^2 - s_2^2}$). In (a) error angle ε and in (b) measured DOP.

The degree of polarisation due to the error in the measured SOP has been plotted in Figure 4.7(b), which shows that the DOP measured (DOP_M) can give values as low as 0.94, although the light is fully polarised. For a SNR of 15 dB, assuming the same error in the optics as used in Figure 4.7, the error in the measured SOP increases and the average angle $\langle \varepsilon \rangle = 2.6^\circ$, as shown in Figure 4.8(a). Figure 4.8(b) shows the measured DOP for a SNR = 15 dB which can now show a minimum value as low as $\sim 90\%$.

The errors ε and DOP_M in Figure 4.7 and Figure 4.8 are calculated from Equation (4.11) and (4.12), by taking the error source values (optics and receiver noise), as fixed. With this in mind, it is possible to show the error in the measured SOP as a function of the error free SOP, however this does not give the worse scenario for the possible error in the SOP and DOP due to the different error sources as defined in Equation (4.11).

A better idea of the expected error in the SOP can be found by using a Monte Carlo simulation with $\pm \Delta a_i$, $\pm \Delta b_3$, and $\pm \Delta d_3$ as the minimum and maximum values of a uniform distribution, and ΔI_i as the standard deviation σ of a zero mean Gaussian.

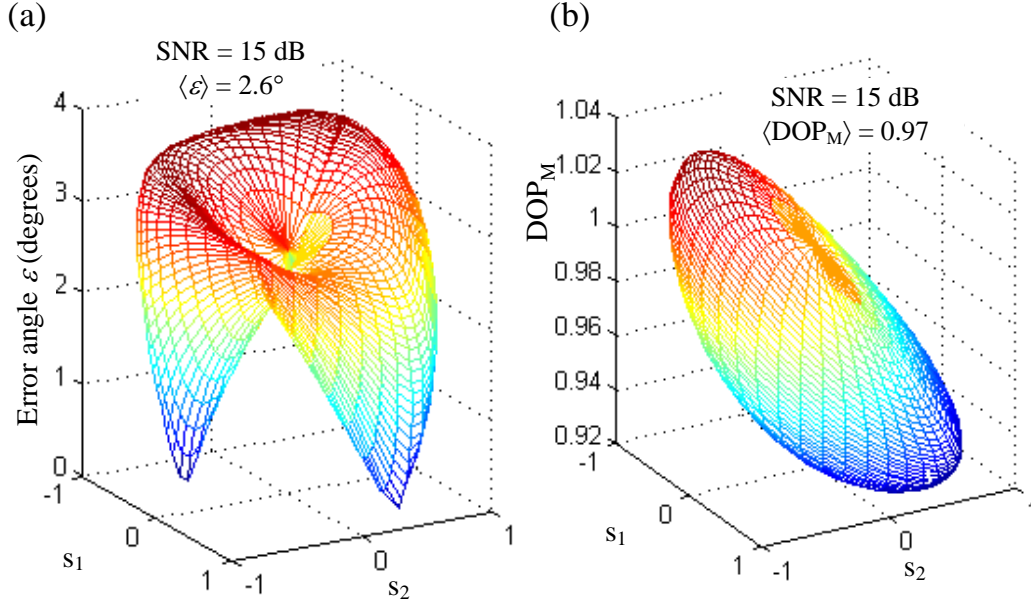


Figure 4.8 Error in measured SOP for fully polarised light with $\Delta a_i = 0.5^\circ$, $\Delta b_3 = 0.5^\circ$ and $\Delta d_3 = \lambda/4 \times 1.5\%$ ($s_3 = \sqrt{1 - s_1^2 - s_2^2}$). In (a) error angle ε and in (b) measured DOP.

Figure 4.9 shows the mean error over all the possible SOPs on the Poincaré sphere from the Monte Carlo simulation, as a function of the maximum - minimum error in Δa_i , Δb_3 , and Δd_3 in (a), and in (b), as a function of the SNR. For a SNR > 20 dB it can be seen in Figure 4.9(a) and (b), that the SOP error (SOP offset) due to the optical elements can be a dominant error source (for error in Δa_i , Δb_3 , and $\Delta d_3 > 0.1^\circ$). For smaller SNRs (< 20 dB) the noise, which causes a spreading of the SOP over time, is the dominant source and the error in the SOP increases exponentially, Figure 4.9(b). The computed error in the SOP from Figure 4.7 to Figure 4.9 has been carried out with fully polarised light, and for depolarised light, the error in the SOP will further increase, as can be seen from Equation (4.10). The error in the SOP can also be expected to increase, if more optical components are used, for example by using quarter waveplates for each channel, due to the additional error caused by the retardation and relative angular position of the $\lambda/4$ plate.

The offset error in the SOP due to Δa_i , Δb_i and Δd_i (for the nominal values of the optical head), can be minimised by calibration as discussed in Section 4.3.4, where in the calibration, the error in the retardation of the $\lambda/4$ plate will then be the dominant error source. The error in the SOP due to the random noise can be minimised by averaging. For the Essex polarimeter without averaging, the NEP of the receiver for 3σ is below -70 dBm, showing that for input

power > -50 dBm, the errors in the optics will be dominant, highlighting again the importance of a good calibration. For a polarimetric OTDR as used in Chapter 7 to measure the backscattered SOP, the incident power is small (e.g. < -60 dBm), and the receiver has to be very fast in order to time resolve the backscattered SOP. In OTDR technology in general, averaging is essential, because the backscattered power is already near the NEP of the receiver, and the error in the SOP using POTDR will be dominated by the receiver noise.

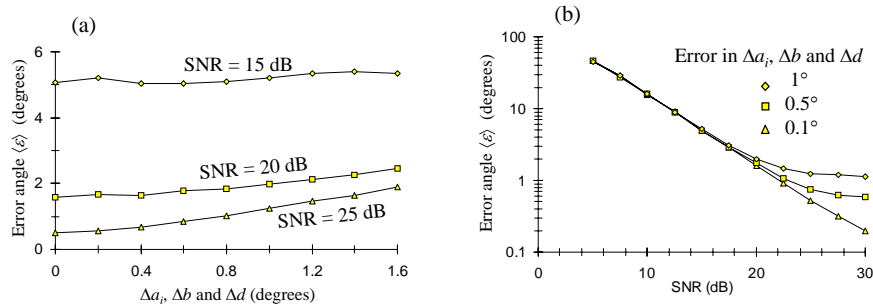


Figure 4.9 Mean value of the error cone angle $\langle \varepsilon \rangle$ using a Monte Carlo simulation with Δa_i , Δb_3 , and Δd_3 taken as the minimum - maximum of a uniform distribution, and ΔI_i as the standard deviation of a Gaussian distribution. In (a), error cone as a function of the error in the optic and in (b), as a function of the SNR in the receiver unit.

4.5 Matrix measurement of optical elements in forward and forward - backward directions

In this section the polarisation matrices of different optical components have been measured where the important results will be to show that the measured components in forward and forward-backward directions with reflection, behave like ideal rotation matrices. Furthermore, it will be shown that for the measured fibres the polarisation matrix for a round trip with reflection shows a rotation vector which is linearly polarised, as would be expected for a reciprocal system.

The polarisation transfer matrix of different elements could be accurately measured by using the polarimeter with open beam input in combination with the polariser - quarter wave plate, to generate well-defined input SOPs (see Figure 4.5). Figure 4.10 shows the set-up for measuring the polarisation matrix of the fibre under test in forward-backward direction, by using a mirror. For the matrix in forward direction the mirror and the beamsplitter, which are mounted on x-y-z stage, are moved out of the optical path.

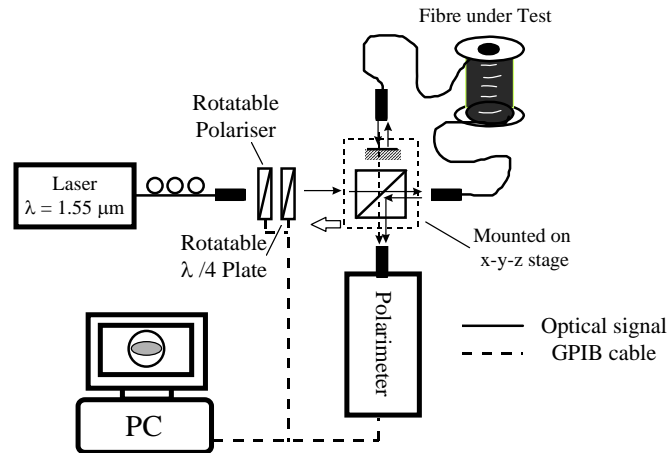


Figure 4.10 Set-up for measuring fibre polarisation matrix in forward and forward-backward directions

The polarisation matrices \mathbf{R}_F in forward direction have been measured for different optical components, and are listed in Table 4.3 for a $\lambda/8$ plate, whose retardation axis has been aligned parallel to the polariser axis, and for a polarisation independent beamsplitter. The matrices have also been measured for two different fibres under test, one loosely lying on the optical table (a few metres length) and the other for fibre spooled on its shipping bobbin (a few hundred metres length). The power for the measurement of the matrices has been maximised in order to keep the error due to noise small (see Figure 4.9). The absolute error in the measured matrix components has been estimated to be $< \pm 0.03$ from repeated measurements, and also, by comparing with the expected nominal values of aligned components, an example is shown in Table 4.3 for the $\lambda/8$ plate. The rotation axis and the rotation angle have been calculated from the eigenvalues of the matrix. The retardation of the $\lambda/8$ plate is as expected within the possible measurement accuracy of 2° . For the so-called polarisation independent beamsplitter, we would expect a unit matrix, but there is some small residual retardation of about $4.7^\circ \pm 2^\circ$ (measured for the straight through direction), keeping the matrix away from a unit matrix. The polarisation matrix of the deflected beam through the beamsplitter showed a unit matrix, which means that for the deflected beam the beamsplitter is, to a good degree, polarisation independent. For the two measured fibre matrices (Fibre I and Fibre II), the retardation has also been given in Table 4.3, but because the actual retardation in these two fibres (containing random perturbation e.g. external stress and twist) can be expected to be larger than π , a multiple of $N\pi$ has to be added to the obtained retardation.

Also in Table 4.3, the forward matrix has been multiplied with its transpose, where we would expect a unit matrix if the fibre behaves like an ideal rotation matrix. This is satisfied for the listed optical components within the expected measurement accuracy. The determinant and the absolute value of the eigenvalue from the matrices are close to one, as would be expected for a rotation matrix.

Forward matrices $\mathbf{R}_F (\pm 0.02)$			
$\lambda/8$ plate	Beamsplitter	Fibre I	Fibre II
$\begin{bmatrix} 0.999 & -0.019 & -0.025 \\ 0.020 & 0.719 & 0.700 \\ -0.013 & -0.706 & 0.712 \end{bmatrix}$	$\begin{bmatrix} 0.97 & 0.012 & 0.007 \\ -0.021 & 1.038 & 0.083 \\ -0.022 & -0.091 & 1.008 \end{bmatrix}$	$\begin{bmatrix} 0.822 & -0.541 & -0.023 \\ 0.16 & 0.194 & 0.971 \\ -0.535 & -0.839 & 0.237 \end{bmatrix}$	$\begin{bmatrix} 0.605 & -0.012 & -0.770 \\ -0.655 & 0.541 & -0.526 \\ 0.480 & 0.856 & 0.326 \end{bmatrix}$
$\det \mathbf{R}_F = 1.01$	$\det \mathbf{R}_F = 1.02$	$\det \mathbf{R}_F = 1.01$	$\det \mathbf{R}_F = 1.01$
Rotation axis (from real eigenvector)			
$[-0.999 \quad 0.006 \quad 0.031]$	$[-0.943 \quad 0.099 \quad -0.318]$	$[-0.899 \quad -0.256 \quad -0.356]$	$[-0.694 \quad 0.641 \quad 0.329]$
Retardation (from complex eigenvalues λ) and $ \lambda = 1$			
$44.5^\circ \pm 2^\circ$ $ \lambda = 1.003$	$< 4.7^\circ \pm 2^\circ$ $ \lambda = 1.03$	$N\pi + 82 \pm 2^\circ$ $ \lambda = 1.01$	$N\pi + 76 \pm 2^\circ$ $ \lambda = 1.02$
$\mathbf{R}_F^T \mathbf{R}_F = \mathbf{I}$ if \mathbf{R}_F is orthogonal			
$\begin{bmatrix} 0.999 & 0.005 & -0.02 \\ 0.005 & 1.014 & 0.002 \\ -0.02 & 0.002 & 0.998 \end{bmatrix}$	$\begin{bmatrix} 0.942 & -0.008 & -0.017 \\ -0.008 & 1.086 & -0.006 \\ -0.017 & -0.006 & 1.023 \end{bmatrix}$	$\begin{bmatrix} 0.989 & 0.036 & 0.009 \\ 0.036 & 1.035 & 0.003 \\ 0.009 & 0.003 & 0.999 \end{bmatrix}$	$\begin{bmatrix} 1.026 & 0.05 & 0.035 \\ 0.05 & 1.026 & 0.004 \\ 0.035 & 0.004 & 0.977 \end{bmatrix}$

Table 4.3 Polarisation matrices of different optical elements in forward direction.

Table 4.4 lists the polarisation matrices measured in forward-backward direction, by using a mirror for the light reflection, and the beamsplitter listed in Table 4.3 to split the launched light from the backreflected light, as shown in Figure 4.10. For the measured matrices $\mathbf{R}_{F,B}$ as listed in Table 4.4, the polarisation rotation matrix of the beamsplitter for the forward direction has been taken into account (Table 4.3), so that the matrices listed are referring to the component under test. The retardation of the $\lambda/8$ waveplate for the forward-reflection-backward measurement $\mathbf{R}_{F,B}$, gives a retardation value of about 90° , which is about double the single way retardation, as would be expected for a round trip through the $\lambda/8$ plate. The matrix $\mathbf{R}_{F,B}$, for just the beamsplitter, shows a matrix close to a unit matrix (polarisation

independent), and is the same matrix as measured for beam deflection through the beamsplitter, which also proves that the SOP on reflection is not altered.

The eigenvectors of the two fibre matrices $\mathbf{R}_{F,B}$ are linearly polarised with the last component in the vector close to zero, as would be expected for one total round trip in the fibre, because the system is reciprocal. The fibre, with respect to one reflection point, behaves as if it possesses only linear birefringence, but because we also know the forward matrix, from Table 4.3 where the eigenvectors are elliptical polarised, we know the fibre contains also twist, and/or, random perturbations. Further, by multiplying $\mathbf{R}_{F,B}$ with its transpose the measured matrices are shown to be well-behaved rotation matrices.

Forward-reflection-backward matrices $\mathbf{R}_{F,B}$ (± 0.02)			
(considering unwanted \mathbf{R}_F caused by the beamsplitter)			
$\lambda/8$ plate	Beamsplitter	Fibre I	Fibre II
$\begin{bmatrix} 1.013 & -0.027 & -0.04 \\ -0.006 & -0.004 & 0.98 \\ -0.01 & -1.01 & 0.005 \end{bmatrix}$	$\begin{bmatrix} 1.015 & -0.016 & -0.046 \\ -0.009 & 0.993 & -0.012 \\ 0.018 & -0.001 & 0.982 \end{bmatrix}$	$\begin{bmatrix} 0.596 & -0.815 & 0.22 \\ -0.754 & -0.425 & -0.455 \\ -0.211 & -0.426 & -0.867 \end{bmatrix}$	$\begin{bmatrix} 0.769 & -0.608 & -0.318 \\ -0.56 & -0.376 & -0.687 \\ 0.294 & 0.694 & -0.647 \end{bmatrix}$
$\det \mathbf{R}_{F,B} = 0.99$	$\det \mathbf{R}_{F,B} = 0.99$	$\det \mathbf{R}_{F,B} = 0.99$	$\det \mathbf{R}_{F,B} = 0.99$
Rotation axis (from real eigenvector)			
$[-1.000 \ 0.008 \ 0.002]$	–	$[0.887 \ -0.461 \ 0.005]$	$[0.926 \ -0.377 \ 0.007]$
Retardation (from complex eigenvalues λ) and $ \lambda = 1$			
$90 \pm 2^\circ$ $ \lambda = 0.997$	–	$N\pi + 150 \pm 2^\circ$ $ \lambda = 0.988$	$N\pi + 129 \pm 2^\circ$ $ \lambda = 0.986$
$\mathbf{R}_{F,B}^T \mathbf{R}_{F,B} = \mathbf{I}$ if $\mathbf{R}_{F,B}$ is orthogonal			
$\begin{bmatrix} 1.026 & -0.017 & -0.046 \\ -0.017 & 1.020 & -0.008 \\ -0.046 & -0.008 & 0.962 \end{bmatrix}$	–	$\begin{bmatrix} 0.967 & -0.076 & 0.029 \\ -0.076 & 1.026 & -0.004 \\ -0.029 & -0.004 & 1.007 \end{bmatrix}$	$\begin{bmatrix} 0.994 & -0.051 & -0.049 \\ -0.052 & 0.993 & 0.003 \\ -0.049 & 0.003 & 0.992 \end{bmatrix}$

Table 4.4 Polarisation matrices of different optical elements in forward-backward direction, with reflection from mirror.